On the detectability of density change in steam-assisted gravity drainage reservoirs using muon tomography

Sara Pieczonka[1], Doug Schouten[2], Oday Dabboor[1], Duncan Osler[3], and Alexander Braun[1,3]

https://doi.org/10.1190/tle39070497.1

Abstract

Muon tomography is applied to realistic density models of a steam-assisted gravity drainage (SAGD) reservoir at 1.25 and 5 years after initial reservoir production. Forward models of muon count and opacity based on the density models are computed, as well as inverse models of the synthetic muon observations for various simulated detector arrays. The results demonstrate that both phases of reservoir development, namely the rising phase and the spreading phase, can be resolved by muon detectors placed 30 m below the bitumen reservoir at 230 m total vertical depth. The total mass change in the reservoir was recovered from the inversion model and differs from the true mass change by 20%–29%. The spatial distribution of density change shows very good agreement in the horizontal direction, while the vertical is less well constrained in this modeled sensor array configuration. The inverse models provide improved insights into reservoir depletion patterns and indicate muon tomography to be an applicable tool for continuous reservoir monitoring. The numerical modeling approach developed herein is able to model a wide range of SAGD reservoir geometries and detector arrays toward planning of optimized monitoring solutions.

Introduction

Muon tomography can detect density anomalies in the subsurface using muon detector arrays located underground. The method has been applied for various applications and targets including greenfield mineral exploration and mining (Schouten and Ledru, 2018; Schouten, 2019), archaeology (Alvarez et al., 1970), and volcanology (Nagamine et al., 1995; Tanaka et al., 2007; Ambrosi et al., 2011; Lesparre et al., 2012; Marteau et al., 2012), to name a few. Herein, we demonstrate the detectability of density anomalies in a steam-assisted gravity drainage (SAGD) reservoir by modeling muon detector arrays and their response through forward and inverse modeling. Using forward-modeled synthetic data based on a realistic SAGD reservoir, an inversion method estimates the density changes across the reservoir. SAGD reservoirs currently are monitored through 4D seismic surveys (Wang, 1997) or resistivity surveys (Ushijima et al., 1999). These methods have limitations in either temporal or spatial resolution, which hinders continuous monitoring at short time scales, e.g., weeks to months. The ultimate goal of this approach is to quantify the capabilities of this method for continuous monitoring of density changes in SAGD reservoirs.

Muon tomography

Muon radiography maps subsurface density by measuring attenuation of cosmic ray muon intensity as muons pass through mass. Muon tomography uses tomographic methods to derive a three-dimensional density distribution underground from multiple muon radiography measurements. A schematic of the muon tomography principles and their use in a SAGD reservoir is shown in Figure 1.

Cosmic ray muons arise from interactions of cosmic rays (predominantly protons and helium nuclei) in the earth's upper atmosphere and can penetrate far into the subsurface. The muon flux that is incident on the earth from all directions at sea level is approximately 1 $cm^{-2}min^{-1}$ (Beringer et al., 2012). Muons lose energy and eventually decay as they pass through matter. The muon intensity underground, denoted by $\mathcal{I}(\mathcal{O},\hat{n})$, can be related to the opacity $\mathcal{O}$ along a path to the surface in the direction $\hat{n}$. Opacity is the mass traversed along the muon path from the surface to the sensor $\mathcal{O}=\int_{\hat{n}}\rho(x,y,z)\,d\ell$, where $\rho(x,y,z)$ denotes the distribution of rock density, and $\mathcal{O}$ is in units of g/cm^2 or meters of water equivalent (m w.e., hectogram/cm^2).

Measurements of cosmic ray muon intensity were first used by George (1955) to measure the overburden of a tunnel and by Alvarez et al. (1970) in search of hidden chambers within pyramids. Over larger spatial scales, muon radiography has been used in volcanology and in deep mineral exploration. In the past decade, the technology has improved both in the resolution and mobility of sensors and computationally through more rigorous and rapid inversion and analysis techniques.

With a muon tracking sensor, trajectories for all muons passing through the sensor are recorded as an image map of muon intensity. Each pixel in these maps represents the measured intensity within a section of solid angle Ωp emanating from an underground sensor up to the surface (Figure 1). The number of muons passing through the detector within a given time period follows a Poisson distribution, so a statistical measure of any deviations between the expected and measured intensity in each pixel can be determined and is represented in the following by $\mathcal{Z}$. Large negative or positive values of $\mathcal{Z}$ indicate regions in which the prior density model is incorrect.

To construct a 3D density distribution from the muon intensity data, an inversion algorithm is used that minimizes a global function ϕ (Menke, 1989):

$$\min_{\rho(x,y,z)}\phi=\min_{\rho(x,y,z)}\left(\phi_D+\beta\cdot\phi_M\right), \tag{1}$$

[1]Queen's University, Department of Geological Sciences and Geological Engineering, Kingston, Ontario, Canada. E-mail: 12sp36@queensu.ca; 16od2@queensu.ca; braun@queensu.ca.
[2]Ideon Technologies Inc., Richmond, British Columbia, Canada. E-mail: doug@ideon.ai.
[3]Queen's University, Department of Physics, Engineering Physics and Astronomy, Kingston, Ontario, Canada. E-mail: 14dmo1@queensu.ca.

where ϕ_D is a data misfit for the muon tomography data compared to an initial model, and ϕ_M is a model objective function that ensures smoothness, namely:

$$\phi_D = \sum_{i \in \text{pixels}} \left(\mathcal{Z}_i - \sum_{j \in \text{voxels}} G_{ij} \rho_j \right)^2 \qquad (2)$$

and

$$\phi_M = \sum_{w=x,y,z} \alpha_w \int_V \left(\frac{\partial \rho}{\partial w} \right)^{q_w} dV + \alpha_r \int_V \rho^p \, dV \,, \qquad (3)$$

where G_{ij} is a sparse sensitivity matrix that relates the $\mathcal{Z}$ of the i^{th} pixel in the radiographic images to the anomalous density ρ_j of the j^{th} voxel in the image volume, α_w is a constant that penalizes roughness in each of the $w = x,y,z$ coordinates, and α_r is a constant that penalizes deviations from a reference model. The aforementioned approach has been implemented in a forward and inversion modeling software to run 3D density models with arbitrary muon detector arrays. The methodology section describes the details of the implementation.

SAGD

In this study, the target for muon tomography is a SAGD reservoir in the McMurray Formation of Alberta, Canada. Monitoring density changes within the reservoir is motivated by two factors: (1) operation and productivity could be enhanced if heavy oil/bitumen and steam could be better localized, and (2) environmental hazards originating from out-of-zone flow could be detected and mitigated. SAGD is one of the enhanced heavy oil recovery methods that requires steam injection to mobilize heavy oil so that it drains into producer wells. SAGD has been developed to efficiently extract immobile bitumen that is situated too deep to be accessed by open mining techniques (Economides and Martin, 2008). Despite the need to monitor productivity and depletion areas within a reservoir, those processes often are inadequately monitored. During the SAGD extraction process, steam is injected into the reservoir through the injection well and mobilizes bitumen so that it drains to an underlying producer well (Figure 2). The bitumen flow must be monitored spatially and temporally to assess recoverability in the reservoir, and to increase production efficiency, as the SAGD process requires considerable energy and water resources. Environmental hazards also must be considered; e.g., bitumen could flow out of the reservoir and into nearby aquifers. Hence, monitoring out-of-zone flow could prevent environmental hazards and mitigate the associated risks.

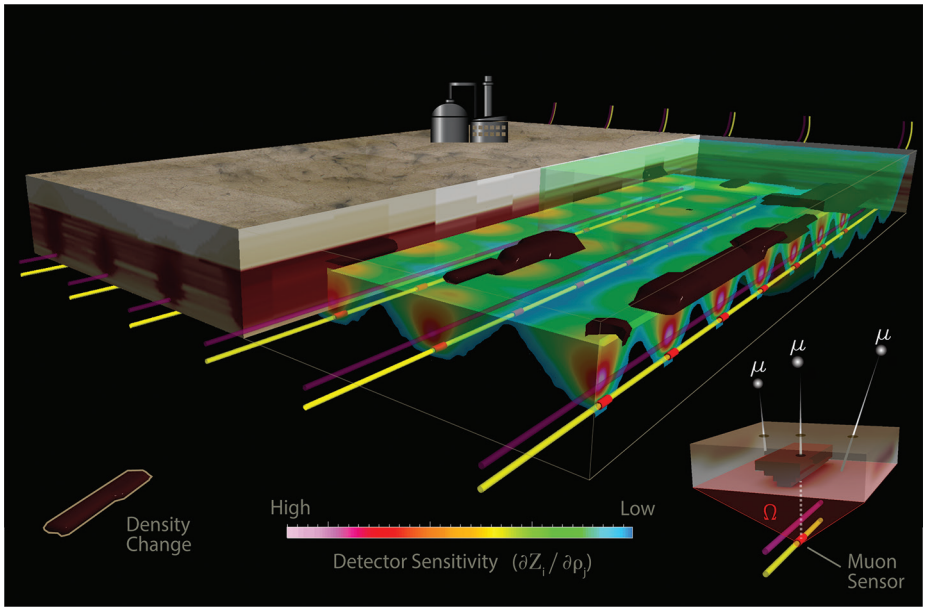

Figure 1. A schematic of a SAGD reservoir with six well pairs and deployed muon detectors shown in red. Inverted cones emanating from the detectors are the effective fields of view of the sensors and are colored in rainbow shades by sensitivity. (The sensitivity cones extend to the surface, as shown in the transparency toward the back.) The sensitivity is greatest nearest to the sensor. Isosurfaces of density change due to reservoir depletion are shown in brown. An insert diagram in the bottom right shows muon tracks (μ) penetrating the ground surface and reaching the sensor within the solid angle (Ω). Some muons are attenuated by the host rock. The central muon passes through a body with a lower density and reaches the detector, which leads to an increased muon intensity in that direction. Note that the figure is not to scale.

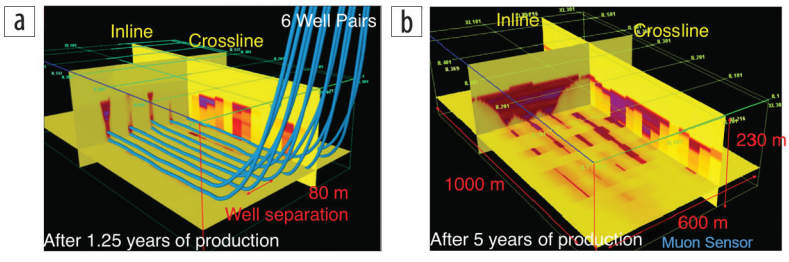

Figure 2. A cartoon of SAGD reservoir models in the McMurray Formation of Alberta. The density model is color-coded with red and purple colors indicating depletion areas. (a) The density distribution along two cross sections after 1.25 years of production and (b) after 5 years. Figure modified after Elliott and Braun (2017).

Current monitoring techniques for bitumen migration include 4D seismic surveys, microseismic surveys, borehole resistivity, temperature and pressure monitoring, and time-lapse gravimetry (Lumley, 2001; Gu et al., 2011; Tondel et al., 2013; Devriese and Oldenburg, 2014; Oloumi et al., 2016; Elliott and Braun, 2017).

Time-lapse seismic surveys provide a comprehensive visualization of the fluid migration, but they are costly and are only conducted every 1 to 3 years. Seismic surveys also have limited sensitivity to changes in fluid content, saturation, and porosity (Devriese and Oldenburg, 2014). Microseismic

monitoring records fracture events, not the fluid migration itself, and is thus an indirect monitoring tool. Borehole monitoring of resistivity, temperature, and pressure is restricted to the area immediately surrounding the wells. Therefore, adequate short-term monitoring to capture the processes of an entire SAGD reservoir is needed. Muon tomography is one of the potential techniques that, in combination with existing methods, could provide a continuous monitoring solution for SAGD reservoirs with adequate spatiotemporal resolution to have tangible benefits for both operational efficiency and environmental risk mitigation.

The major objective of this study is to determine the detectability of density anomalies in a real SAGD reservoir at different stages of production through muon tomography. Specifically, we analyze requirements for muon sensor arrays, the sensitivity of those arrays to identify depletion volumes in a realistic SAGD reservoir, and inversion model limitations at different production stages of the reservoir.

Methodology

Muon forward and inverse modeling. In this study, forward modeling is performed using modeling software developed by Ideon Technologies Inc. (formerly known as CRM Geotomography Technologies Inc.) and described in Schouten and Ledru (2018) and Schouten (2019). The muon intensity $\mathcal{I}(\mathcal{O},\hat{n})$ is stored in a multidimensional lookup grid for various media. The expected number of muons to be detected within a given pixel p of a detector image map is determined by

$$\mathcal{N} = \Delta t \int_{\Omega_p} \underbrace{\left(\int_0^\infty D_\mu(E,\theta) \cdot p(E;\mathcal{O}) dE \right)}_{=\mathcal{I}(\mathcal{O},\hat{n})} \alpha(\hat{n}) d\Omega , \qquad (4)$$

where Δt is the exposure time of the sensor, $D_\mu(E,\theta)$ is the sea-level muon momentum spectrum as a function of the muon energy E and angle θ with respect to vertical, $p(E;\mathcal{O})$ is the probability for a muon with energy E to survive through a certain opacity $\mathcal{O}$, and $\alpha(\hat{n})$ incorporates the sensor acceptance and detection efficiency as a function of the muon trajectory. Note that muon scattering is ignored in this formulation but, for reasonable depths, the dominant imaging blurring is due to Poisson statistics, so this is a valid approximation.

The inverse problem is posed by defining the sensitivity matrix G for the linearized problem,

$$G_{ij} = \frac{\partial \mathcal{Z}_i}{\partial \rho_j} \approx \frac{\Delta t \int_{\Omega_{pi}} \alpha(\hat{n}) \left(\ell_j(\hat{n}) \cdot \frac{d\mathcal{I}(\mathcal{O},\hat{n})}{d\mathcal{O}} \right) d\Omega}{\sqrt{\mathcal{N}}} , \qquad (5)$$

where $\ell_j(\hat{n})$ is the path length of a straight ray along $\hat{n}$ through the j^{th} voxel, and the approximation is in the Gaussian limit of the Poisson distribution.

Model input. The density data that serve as the input to the forward model and the truth comparison herein for the inversion models are from a real SAGD reservoir located in the Athabasca region of Alberta, Canada. The density data provided by the operator were compiled from geologic and geophysical observations including well and core logs, 3D seismic, log analysis, reservoir and geologic modeling, and regional comparisons. The density data were provided at 2 × 2 × 2 m spatial density, at three time intervals after initial production (AIP) — 0, 1.25, and 5 years.

The average absolute density of the targeted formation is 2.16 g/cm^3, and the density ranges between 2.04 and 2.62 g/cm^3. The area under production is approximately 600 × 1000 m with a targeted depth of 200 m total vertical depth (TVD). Six well pairs are located at 230 m TVD with an approximate crossline well separation of 80 m between pairs. The density models used herein have a voxel size of 2 × 2 × 2 m and were forward modeled with various muon detector arrays to quantify the sensitivity of the arrays toward density anomalies.

The two time intervals AIP represent two major phases of reservoir development: the rising phase (1.25 AIP) and the spreading phase (5 AIP). During the rising phase, the reservoir is only partially heated close to the injector wells, and bitumen depletion occurs along the wells but does not occur in areas between them. It is visible through density changes along vertical curtains over the injector wells (Figure 2). The spreading phase occurs later in the production cycle when the reservoir as a whole is sufficiently heated. During this phase, the heated volume has expanded across the well pairs and leads to more homogeneous depletion patterns except in those areas where lithologic variations prevent the steam from contacting the bitumen. Both phases of reservoir development are tested herein to identify the applicability of muon tomography throughout the SAGD reservoir life cycle.

Model parameters. The muon detector arrays implemented in the models were designed to fit the requirements of the specific SAGD reservoir geometry, assuming that detectors can be placed in the horizontal wells beneath the reservoir layer. (Factors that need to be addressed for this assumption in a real-world scenario include high temperatures within the producing wells and the specific size of the wells at different field sites.) This assumption leads to a crosswell spacing of 80 m, or 160 m if detectors are only installed in every other well pair. A sensitivity study revealed that it is necessary to place detectors in every available well. Otherwise, parts of the reservoir volume are not monitored due to the limited visibility area of the detectors. Hence, the crosswell spacing of the detectors was set to 80 m in this model, and this configuration includes 98% of the reservoir within the view of the sensors. The sensitivity of the sensors to the reservoir volume is shown in Figure 1. The depth of the detectors was fixed to 230 m TVD. The flux of muons through all detectors at 230 m is estimated to be approximately 190 muons/minute, and the exposure time of the sensors was set to 90 days. The data become more resolved with time as muon counts increase. This time interval is sufficient to smooth out Poisson noise, but meaningful results can be obtained in shorter time frames down to weeks. The sensors in this modeling study are designed to fit inside an "HQ"-sized wellbore and are 10 cm in diameter and 3 m in length. Customizations are required for a real-world scenario to accommodate the temperature and size logistics of the encapsulating borehole. The muon intensity is highest near the vertical direction for horizontally

oriented sensors because there is less depth to traverse from this direction. Muons can be detected from all angles above the sensors, but due to the drop off in intensity away from a zenith of 0°, an effective viewing angle of a single sensor is approximately 50° from the vertical. The α_r term in equation 3 is set to zero so that no reference model is included and no prior geologic information is added. The models shown and discussed in the results represent unconstrained inversions.

Results

The inversion modeling results are shown for 6 × 6 × 6 m voxels using 180 sensors spread evenly throughout the six well pairs. Synthetic muon data were produced through forward modeling of density values from the SAGD reservoir for two scenarios: a reference model "REF0" (before production started) and depleted models "DEP1" and "DEP5" (after 1.25 and 5 years of operation, respectively) relative to REF0. The forward-modeled data were inverted to test comparability between the inversion results labeled "CRM" (cosmic ray muon) and the true density models. The results are presented first for DEP1 and finally for DEP5. A scatter plot shows the density change for the true and inverted models by voxel location and allows for a comparison between the inversion and the true density models. The 3D visualizations show the entire model density distribution as the background volume, and the specific density change isosurfaces are highlighted in blue colors for contrast. Isosurfaces are contoured at the peripheral 7%, 5%, and 3% of the maximum density change in the depleted data compared to the reference data for both the true and inversion models to show an unbiased comparison between the truth and the inversion. The inversion demonstrates the ability to localize the anomalies despite having different magnitudes.

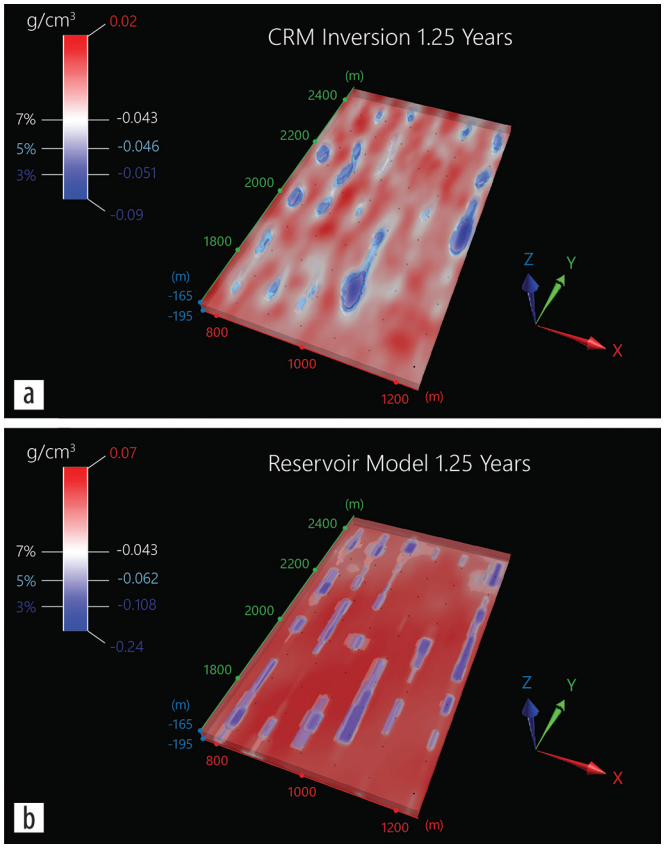

Figure 3. Inversion results at the 1.25-year time interval after initial production (DEP1). (a) The CRM inversion model and (b) the true model. Both models are contoured at their respective peripheral 7%, 5%, and 3% of the density change from time 0 (REF0) data in g/cm³.

Results after 1.25 years. Inversion results after 1.25 years of production are shown in Figure 3, compared with the true reservoir model at the same time after initial production. Both the inversion and true model contours are shown within the volume in its entirety. The inversion results are contoured at three intervals of depletion to show localization ability and precision in spatial resolution. The density depletion areas are localized above the wellbores correlating with the rising phase of reservoir depletion. The inversion model shows depletion areas that spatially correlate well with the true model and correctly localizes anomalies of high depletion rates along the wells. The maximum density change from the inversion is −0.09 g/cm³ with a mean density change of −0.0144 g/cm³. The maximum density change in the true model is −0.24 g/cm³ with a mean density value of −0.0107 g/cm³. The true model shows a greater range in density values, and the mean change in densities between both models differs by 0.0037 g/cm³ or 29% (relative). The 2D histogram in Figure 4 shows the density change across all voxels within the reservoir for both models. It can be seen that the density change is correlated for the models, but the vertical bars, especially around (0,0), show vertical smearing in the inversion. This is a consequence of the inversion algorithm being unable to constrain the magnitude of density change and the vertical location at the same time, which is inherent in every inverse modeling problem. In this unconstrained inversion, the smearing of depletion occurs along the muon trajectories, and further constraints must be applied to mitigate this effect.

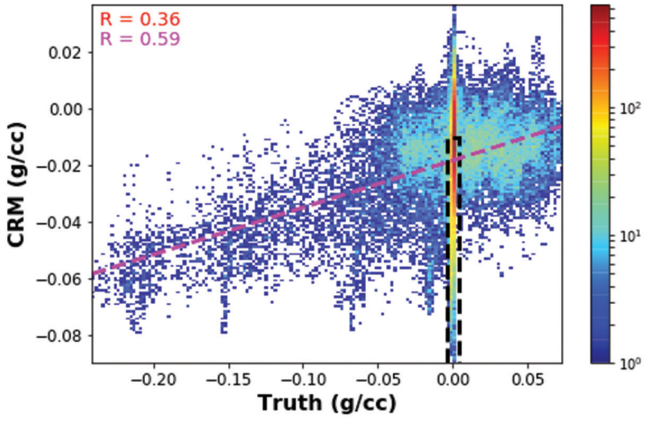

Figure 4. A 2D histogram of true versus CRM inversion density change at equivalent voxel locations in g/cm³ at the 1.25-year time interval after initial production. The data are colored by number of voxels at the axes' density change values. The Pearson correlation coefficient R value for all data within the reservoir is shown in red. The black rectangle outlines the data that show zero depletion in the truth but varying depletion in the inversion model. These data represent vertical smearing in the inversion. The spatial location of these voxels is shown in Figure 5. The R value shown in pink is calculated with these voxels removed from the data set.

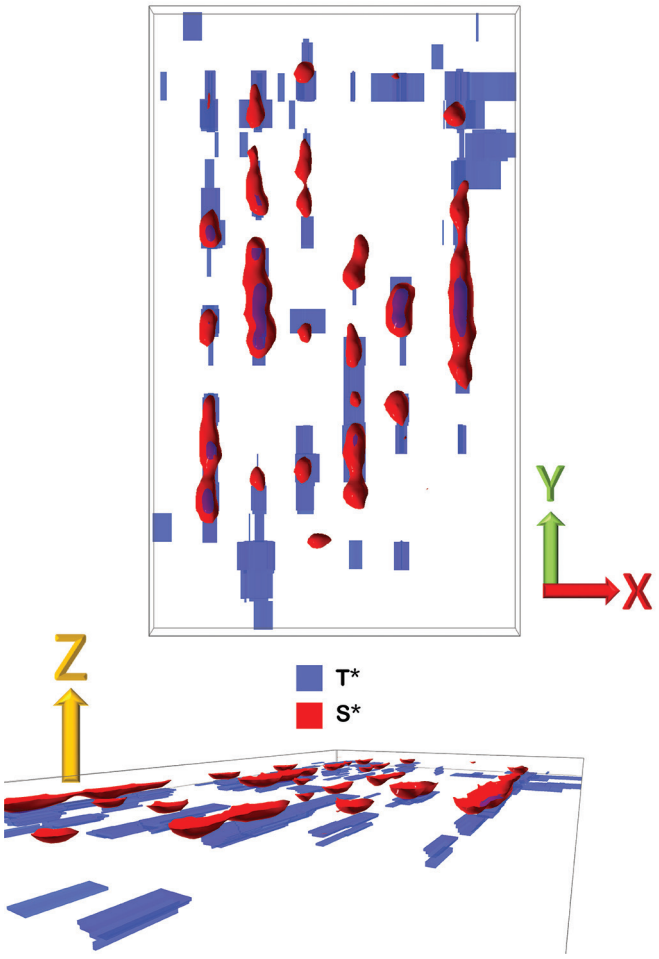

Figure 5. The spatial location of vertical smearing in the inversion model shown in plan view (top) and in an oblique zoomed view (bottom). The set of voxels with true depletion is shown in blue (T*), and locations of vertical smearing (voxel locations in the black rectangle in Figure 4) are shown in red (S*). The vertical smearing is shown here to occur at locations directly above the well pairs.

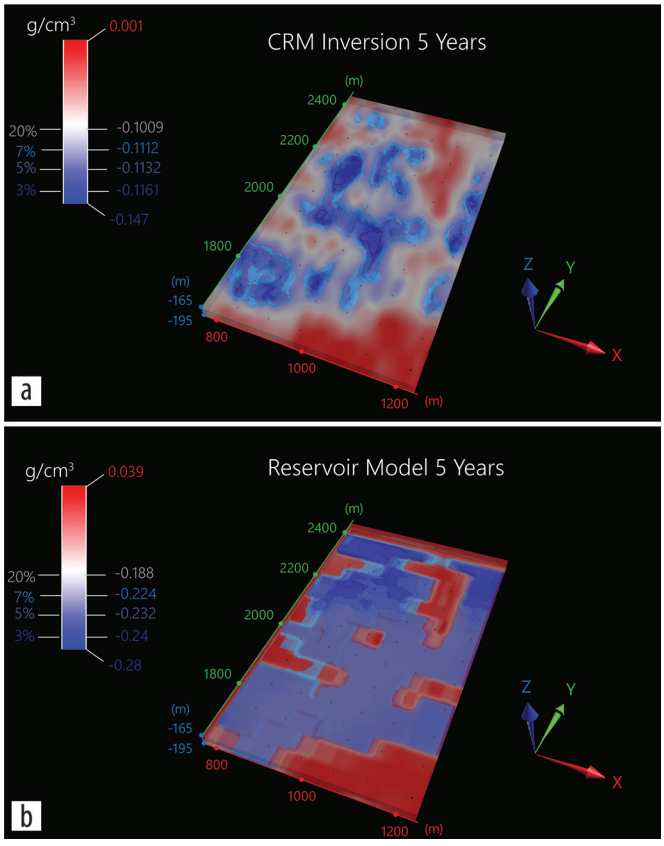

Figure 6. Inversion results at the 5-year time interval after initial production (DEP5). (a) The CRM inversion model and (b) the true model. Both models are contoured at their respective peripheral 7%, 5%, 3% of the density change from time 0 (REF0) data in g/cm³.

To demonstrate this concept further, the voxels highlighted in the black box in Figure 4 are shown spatially in Figure 5. Those voxels that have zero depletion in the truth data but that show varying depletion in the inversion are shown as red surfaces, which arise in the inversion above the true depletion (blue). These voxels are located above the well pairs, showing that the inversion is correctly localizing the lateral location of the depletion but smearing the depletion out in the vertical direction. Removing these voxels shows an increase in the Pearson correlation coefficient (the red versus pink R values) in Figure 4.

The total mass change is 417 kt for the true model versus 560 kt for the inverse model. The simulated muon array is able to resolve the location and relative magnitude of density change caused by bitumen depletion during the rising phase very well. Most importantly, it detected the two areas in the reservoir where no depletion occurred (northeastern and southeastern corners of the reservoir along the fifth well pair; x_1 = 1120, y_1 = 1750, and x_2 = 1120, y_2 = 2250, and the southwestern section along the second well pair at x_3 = 960, y_3 = 1900).

Results after 5 years. Inversion results after 5 years of steam injection (DEP5) are shown in Figure 6, compared with the true reservoir model at the same time AIP. As with DEP1, both models show the entire volume of density change and are contoured at the same contour intervals of 7%, 5%, and 3% of the peripheral maximum density change from initial production. The spread of depletion in blue between the wells indicates the transition into the spreading phase. At this stage, most of the reservoir experiences depletion as the steam chamber reaches maximum height and spreads laterally between wells. Viewing from the surface reveals that individual well pairs can no longer be distinguished as the spreading phase covers the rising phase volumes. The inversion model shows similar depletion patterns to the true model, highlighting a large area of low depletion in the central northeast sector along the fifth well and also the lack of depletion entirely in the southeast corner of the reservoir, similar to the status in DEP1 (Figure 3). The inversion even localizes smaller areas of low or no depletion such as in spots along the westernmost well and two isolated spots along the third and fourth wells (approximately x_1 = 900–1000). The maximum density change in the inversion model is –0.14 g/cm³ with a mean density change of –0.064 g/cm³. The maximum density change in the true model is –0.28 g/cm³ with a mean density value of –0.0524 g/cm³. The true model still shows a greater range in density values, and the mean change in densities between both models differs by 0.012 g/cm³ or 20% (relative).

The total mass change is 2040 kt for the true model and 2491 kt for the inverse model. As in DEP1, the DEP5 inverse

model creates lower magnitudes of density change than the true model, although the mean density change (and overall mass change) is closer at 5 years. While the depletion patterns are well represented, the magnitude of density change remains less well constrained. This arises from the nonuniqueness of the inversion algorithm, especially in this particular sensor configuration where the sensors are directly below the wells.

Discussion

The discussion section will describe (1) the strength and weaknesses of the approach used herein for SAGD reservoir monitoring, (2) the number of muon detectors in the array, (3) the nonuniqueness of the inversion results, and (4) how other methods could be incorporated to overcome the limitations.

The results presented here demonstrate that muon tomography may be an excellent tool to detect density anomalies in SAGD reservoirs even at scales that often are not detectable by other geophysical methods, such as potential field methods or seismic imaging. The horizontal position of depletion volumes in the inverse models compares well with the true models. However, the vertical position is less well constrained in this modeled sensor configuration. The magnitude of density change is generally lower for the inverse models compared to the true models. This is an artifact of the inversion algorithm associated with the nonuniqueness of the solution. As the inversion algorithm minimizes the objective function, the density values are changed to reach an improved fit. The density changes are not well constrained in the vertical by the muon detectors, which leads to density anomalies being smeared across the depth range of the reservoir above the sensors. There are two complementary options to improve this: (1) include auxiliary information about the density distribution (e.g., from gravimetry, seismic, or geologic information), or (2) optimize the location of the detectors to improve the vertical resolution, such as by using sensors in vertical boreholes rather than a singular depth as in the horizontal array used in this study. This may require more muon detectors and potentially additional or even dedicated boreholes for muon tomography. A logical next step to improve the result is to apply constraints that include weighting matrices, known geologic information such as assay data, and to implement vertical sensor arrays. The addition of the vertical array also could mitigate the issue of temperature limitations on the sensors, as the vertical boreholes can be drilled between the well pairs.

The localization of depletion volumes is probably the most robust attribute of muon tomography and inversion and would allow for improved decisions about steam injection rates per well or production changes. This method also would be able to localize out-of-zone flow, as indicated by the robustness of the inversion models. This approach could detect low (or zero) depletion areas across the life cycle of the reservoir, both during the rising and the spreading phases on a quasi-continuous basis (i.e., 90 days or less with additional muon sensors).

To successfully localize out-of-zone flow, the depletion chamber geometry must be further constrained to minimize spurious smearing. With the sensor array used in this study and representing an unconstrained scenario, the lateral resolution is already high enough to model meter-scale depletion. If the aforementioned constraints are used to improve the vertical resolution, it is reasonable to anticipate that the inversion is adequate to identify possible leakage areas. With appropriate detector configurations and additional inversion constraints, muon tomography could be used to detect the leakage of contaminants exiting the reservoir.

The mean density change and the total mass change between inverse models and true models is reasonably well constrained, which can be expected, but the range of density changes is different. This could only be overcome by using more constraints for the inverse model, e.g., through limiting the volume in which density can change in the inversion process. In this sense, the "blind" inversion algorithm used herein is conservative because no constraints were imposed on the solution from the known geometry of the depletion zones as emanating from the injection wells.

A muon detector's field of view is an upside-down cone, which limits its sensitivity to a very narrow region near the detector and a wide region near the surface (Figure 1). The viewing cones of neighboring detectors may overlap but often only in the upper part of the cone if sensors are far apart. A second related obstacle is the geometric ambiguity, as density anomalies anywhere along a muon trajectory between the surface and the underground sensor in one direction will have the same effect on the observation. Therefore, multiple views from different sensors are needed to triangulate the anomaly.

While seismic surveys are the conventional choice for monitoring bitumen depletion in SAGD reservoirs (Lumley, 2001; Devriese and Oldenburg, 2014; Oloumi et al., 2016), they are expensive and labor intensive, and they suffer from ambiguities in interpretation because they do not directly measure density. A gravimetric study by Elliott and Braun (2017) using synthetic data from modeling super-conducting gravimetry and gradiometry shows that gravity data could be used to detect density changes in a SAGD reservoir over time caused by fluid migration and depletion. While gravimetric data can also measure density directly and have high resolution close to the sensor, they suffer from decreased resolution with depth. Muon tomography can provide high-resolution average densities in a constrained direction, but it lacks in spatial resolution along the raypaths. Muon tomography is also limited by the number and placement of sensors and campaign duration, which leads to an underdetermined inversion problem. A joint inversion between gravity and muon data could complement each other because they both measure the same parameter and can better constrain the true density changes (Barnoud et al., 2019; Cosburn et al., 2019; Lelièvre et al., 2019). A joint inversion between gravimetric and muon data was introduced by Davis and Oldenburg (2012) and can be performed in Ideon Technologies' inversion code. It was also described by Nishiyama et al. (2014) and was established quantitatively for realistic heterogeneous models by Jourde et al. (2015). Studies by Nishiyama et al. (2017) and Rosas-Carbajal et al. (2017) successfully use joint inversions to model lava domes using real observations.

Conclusion

This study demonstrates the detectability of SAGD reservoir depletion patterns through muon tomography. Forward and inverse modeling was applied to realistic SAGD reservoir density models for time intervals 1.25 and 5 years AIP. Forward modeling of a muon detector array response to density changes revealed that approximately 180 detectors are needed in the six well pairs covering a 600 by 1000 m large reservoir to resolve depletion volumes for individual well pairs at short time intervals of 90 days. An important advantage of muon tomography is that once the sensors are installed, they remain there for continuous surveying with little or no maintenance. So even with a large number of sensors, this method is expected to be competitive in cost to current monitoring techniques within the first survey campaign. Further, this study was completed with a short exposure time of 90 days, but the number of sensors can be decreased in exchange for longer exposure times (approximately one-third of sensors for a 120-day survey).

After 1.25 years of operation, the results of the inversion model clearly show where the reservoir was depleted and areas that did not experience any depletion. After 5 years of production, the results demonstrate that the reservoir was further depleted, including between the well pairs. Both results indicate that muon tomography could provide important depletion parameters toward optimized operations. Firstly, operators may use the results to identify regions and well pair segments that do not show any density change and therefore do not produce efficiently. Those segments of the reservoir could be removed from steam injection to save energy costs. Secondly, environmental risks associated with out-of-zone flow could be detected and mitigated early, compared to less frequent 4D seismic monitoring.

Muon tomography is applicable to monitor SAGD reservoirs across realistic reservoir depth ranges of several hundred meters and may provide a marked improvement in spatial resolution in detecting density changes. Besides the potential improvements shown here, SAGD reservoir monitoring could benefit from a joint inversion that incorporates surface gravity, gravity gradiometry, seismic, and muon tomography. The differing sensitivities of these methods can provide a complementary combination to constrain the inversion model and fill in blind zones and shallow target depths that muon data may be lacking due to lack of visibility or resolution. Operational constraints such as well diameter and high temperatures likely make dedicated muon tomography monitoring wells a better option than adding the detectors to the producer well due to the harsh environmental conditions in the producer well and logistic constraints. Nevertheless, the results presented here clearly show the potential of this innovative monitoring approach for SAGD and other enhanced oil recovery methods. TLE

Data and materials availability

Data associated with this research are confidential and cannot be released.

Corresponding author: 12sp36@queensu.ca

References

Alvarez, L. W., J. A. Anderson, F. El Bedwei, J. Burkhard, A. Fakhry, A. Girgis, A. Goneid, et al., 1970, Search for hidden chambers in the pyramids: Science, **167**, no. 3919, 832–839, https://doi.org/10.1126/science.167.3919.832.

Ambrosi, G., F. Ambrosino, R. Battiston, A. Bross, S. Callier, F. Cassese, G. Castellini, et al., 2011, The MU-RAY project: Volcano radiography with cosmic-ray muons: Nuclear Instruments and Methods in Physics Research Section A: Accelerators, Spectrometers, Detectors and Associated Equipment, **628**, no. 1, 120–123, https://doi.org/10.1016/j.nima.2010.06.299.

Barnoud, A., V. Cayol, V. Niess, C. Cârloganu, P. Lelièvre, P. Labazuy, and E. Le Ménédeu, 2019, Bayesian joint muographic and gravimetric inversion applied to volcanoes: Geophysical Journal International, **218**, no. 3, 2179–2194, https://doi.org/10.1093/gji/ggz300.

Beringer, J., J.-F. Arguin, R. M. Barnett, K. Copic, O. Dahl, D. E. Groom, C.-J. Lin, et al., 2012, Review of particle physics: Physical Review D, **86**, no. 1, https://doi.org/10.1103/PhysRevD.86.010001.

Cosburn, K., M. Roy, E. Guardincerri, and C. Rowe, 2019, Joint inversion of gravity with cosmic ray muon data at a well-characterized site for shallow subsurface density prediction: Geophysical Journal International, **217**, no. 3, 1988–2002, https://doi.org/10.1093/gji/ggz127.

Davis, K., and D. W. Oldenburg, 2012, Joint 3D of muon tomography and gravity data to recover density: ASEG Extended Abstracts, **2012**, no. 1, 1–4, https://doi.org/10.1071/ASEG2012ab172.

Devriese, S. G. R., and D. W. Oldenburg, 2014, Enhanced imaging of SAGD steam chambers using broadband electromagnetic surveying: 84th Annual International Meeting, SEG, Expanded Abstracts, https://doi.org/10.1190/segam2014-1247.1

Economides, M. J., and T. Martin, 2008, Modern fracturing: Enhancing natural gas production: Gulf Publishing Co., 116–125.

Elliott, E. J., and A. Braun, 2017, On the resolvability of steam assisted gravity drainage reservoirs using time-lapse gravity gradiometry: Pure and Applied Geophysics, **174**, no. 11, 4119–4136, https://doi.org/10.1007/s00024-017-1636-5.

George, E. P., 1955, Cosmic rays measure overburden of tunnel rays measure overburden of tunnel: Commonwealth Engineer, 455–457.

Gu, F., M. Y. S. Chan, and R. Fryk, 2011, Geomechanical-data acquisition, monitoring, and applications in SAGD: Journal of Canadian Petroleum Technology, **50**, no. 6, 9–21, https://doi.org/10.2118/145402-PA.

Jourde, K., D. Gibert, and J. Marteau, 2015, Improvement of density models of geological structures by fusion of gravity data and cosmic muon radiographies: Geoscientific Instrumentation: Methods and Data Systems, **4**, 177–188, https://doi.org/10.5194/gi-4-177-2015.

Lelièvre, P. G., A. Barnoud, V. Niess, C. Carloganu, V. Cayol, and C. G. Farquharson, 2019, Joint inversion methods with relative density offset correction for muon tomography and gravity data, with application to volcano imaging: Geophysical Journal International, **218**, no. 3, 1685–1701, https://doi.org/10.1093/gji/ggz251.

Lesparre, N., D. Gibert, J. Marteau, J.-C. Komorowski, F. Nicollin, and O. Coutant, 2012, Density muon radiography of La Soufrière of Guadeloupe volcano: Comparison with geological, electrical resistivity and gravity data: Geophysical Journal International, **190**, no. 2, 1008–1019, https://doi.org/10.1111/j.1365-246X.2012.05546.x.

Lumley, D. E., 2001, Timelapse seismic reservoir monitoring: Geophysics, **66**, no. 1, 50–53, https://doi.org/10.1190/1.1444921.

Marteau, J., D. Gibert, N. Lesparre, F. Nicollin, P. Noli, and F. Giacoppo, 2012, Muons tomography applied to geosciences and volcanology: Nuclear Instruments & Methods in Physics Research Section A: Accelerators, Spectrometers, Detectors and Associated Equipment, **695**, 23–28, https://doi.org/10.1016/j.nima.2011.11.061.

Menke, W., 1989, Geophysical data analysis: Discrete inverse theory, revised ed.: Elsevier.

Nagamine, K., M. Iwasaki, K. Shimomura, and K. Ishida, 1995, Method of probing inner-structure of geophysical substance with the horizontal cosmic-ray muons and possible application to volcanic eruption prediction: Nuclear Instruments & Methods in Physics Research Section A: Accelerators, Spectrometers, Detectors and Associated Equipment, **356**, no. 2–3, 585–595, https://doi.org/10.1016/0168-9002(94)01169-9.

Nishiyama, R., S. Miyamoto, S. Okubo, H. Oshima, and T. Maekawa, 2017, 3D density modeling with gravity and muon-radiographic observations in Showa-Shinzan lava dome, Usu, Japan: Pure and Applied Geophysics, **174**, no. 3, 1061–1070, https://doi.org/10.1007s00024-016-1430-9.

Nishiyama, R., Y. Tanaka, S. Okubo, H. Oshima, H. K. M. Tanaka, and T. Maekawa, 2014, Integrated processing of muon radiography and gravity anomaly data toward the realization of high-resolution 3-D density structural analysis of volcanoes: Case study of Showa-Shinzan lava dome, Usu, Japan: Journal of Geophysical Research. Solid Earth, **119**, no. 1, 699–710, https://doi.org/10.1002/2013JB010234.

Oloumi, D., K. K. Chan, P. Boulanger, and K. Rambabu, 2016, SAGD process monitoring in heavy oil reservoir using UWB radar techniques: IEEE Transactions on Microwave Theory and Techniques, **64**, no. 6, 1884–1895, https://doi.org/10.1109/TMTT.2016.2561926.

Rosas-Carbajal, M., K. Jourde, J. Marteau, S. Deroussi, J.-C. Komorowski, and D. Gibert, 2017, Three-dimensional density structure of La Soufrière de Guadeloupe lava dome from simultaneous muon radiographies and gravity data: Geophysical Research Letters, **44**, no. 13, 6743–6751, https://doi.org/10.1002/2017GL074285.

Schouten, D., 2019, Muon geotomography: Selected case studies: Philosophical Transactions of the Royal Society A: Mathematical, Physical and Engineering Sciences, **377**, no. 2137, 20180061, https://doi.org/10.1098/rsta.2018.0061.

Schouten, D., and P. Ledru, 2018, Muon tomography applied to a dense uranium deposit at the McArthur River Mine: Journal of Geophysical Research. Solid Earth, **123**, no. 10, 8637–8652, https://doi.org/10.1029/2018JB015626.

Tanaka, H. K. M., T. Nakano, S. Takahashi, J. Yoshida, M. Takeo, J. Oikawa, T. Ohminato, et al., 2007, High resolution imaging in the inhomogeneous crust with cosmic-ray muon radiography: The density structure below the volcanic crater floor of Mt. Asama, Japan: Earth and Planetary Science Letters, **263**, no. 1-2, 104–113, https://doi.org/10.1016/j.epsl.2007.09.001.

Tondel, R., S. Dummong, H. Schutt, A. Ducrocq, R. Godfrey, J. Ingham, and D. LaBrecque, 2013, Reservoir monitoring in oil sands using a permanent cross-well system: Status and results after 18 months of production: Second EAGE Workshop on Permanent Reservoir Monitoring, https://doi.org/10.3997/2214-4609.20131315.

Ushijima, K., H. Mizunaga, and T. Tanaka, 1999, Reservoir monitoring by a 4-D electrical technique: The Leading Edge, **18**, no. 12, 1422–1424, https://doi.org/10.1190/1.1438242.

Wang, Z., 1997, Feasibility of time-lapse seismic reservoir monitoring: The physical basis: The Leading Edge, **16**, no. 9, 1327–1330, https://doi.org/10.1190/1.1437796.